



Breast cancer diagnosis with a microwave thermoacoustic imaging technique—a numerical approach

M. Soltani^{1,2,3,4,5} · Reza Rahpeima⁶ · Farshad Moradi Kashkooli¹

Received: 29 May 2018 / Accepted: 2 February 2019 / Published online: 27 March 2019
© International Federation for Medical and Biological Engineering 2019

Abstract

Microwave-induced thermoacoustic imaging (MITAI) is an imaging technique with great potential for detecting breast cancer at early stages. Thermoacoustic imaging (TAI) combines the advantages of both microwave and ultrasound imaging techniques. In the current study, a three-dimensional novel numerical simulation of TAI phenomenon as a multi-physics problem is investigated. In the computational domain, a biological breast tissue including three different tissue types along with a tumor is placed in a tank containing castor oil and is irradiated by a 2.45-GHz pulsed microwave source from a rectangular waveguide. The generated heat in the biological tissue due to the electromagnetic wave irradiation and its corresponding pressure gradient in the tissue because of the temperature variations are evaluated. Also, capability of the MITAI process with respect to the tumor location and size is investigated. To identify the required power level needed for producing thermoacoustic signals, different power levels of microwave sources are investigated. The study's results demonstrate a minuscule increase in temperature as a result of the absorption of pulsed microwave energy (for example, a maximum of 0.002472 °C temperature increase in tumor with 1 cm diameter which is located in fatty tissue of breast are obtained due to an excitation pulse of 1000 W, 1 ms). This small temperature variation in the tumor produces several kilopascals of pressure variations with maximum of 0.584016 kPa in tumor. This pressure variation will produce acoustic signals, which can be detected with an array of transducers and be used for image construction. Results demonstrate that the location of tumor in breast plays a vital role on the detecting performance of MITAI. Also, it is shown that very small tumors (with the diameter of 0.5 cm) can also be detected using MITAI technique. These simulations and procedures can be used for determining the amount of produced pressure variation, the acoustic pressure magnitude, and other complicated geometries.

Keywords Thermoacoustic imaging (TAI) · Thermoacoustic tomography · Breast tumor · Early detection · Microwave

1 Introduction

Breast cancer is the second most common cancer in the world after lung cancer [11]. Statistical data has shown a deep penetration of this type of cancer in females compared to males; less than 1% of all breast cancers belong to males, whereas the remaining 99% has been observed in females [27]. Although there are huge amounts of dissimilarities related to breast cancer driver genes between male and female patients, which may compel practitioners to prescribe different necessary treatment protocols [19], it seems that most cancer symptoms are similar in a diagnostic way for both gender categories [48]. Practical reasons, such as rarity and a low index of suspicion for male breast cancer, are recognized as causes for a mean delay of 6–10 months in performing a diagnostic procedure [30]. This situation might clarify that, like other types of cancers, there is a serious demand for timely diagnosis of breast cancer, regardless of male or female types of breast cancer.

✉ M. Soltani
msoltani@uwaterloo.ca

¹ Department of Mechanical Engineering, K. N. Toosi University of Technology, Tehran, Iran
² Advanced Bioengineering Initiative Center, Computational Medicine Center, K. N. Toosi University of Technology, Tehran, Iran
³ Cancer Biology Research Center, Cancer Institute of Iran, Tehran University of Medical Sciences, Tehran, Iran
⁴ Department of Electrical and Computer Engineering, University of Waterloo, Waterloo, Ontario, Canada
⁵ Centre for Biotechnology and Bioengineering (CBB), University of Waterloo, Waterloo, Ontario, Canada
⁶ Department of Aerospace Engineering, K. N. Toosi University of Technology, Tehran, Iran

One way for tracking early-stage breast cancer is X-ray mammography. In a typical X-ray mammography system, an X-ray imager is used to take a projection X-ray image [18]. However, this technique is inefficient in early detection of breast cancer because in X-ray mammography, identifying cancerous tissues highly depends on density variation. Such variation, however, is not significant, or may not be applicable, for detecting or tracking a tumor's evolution since its initial stages [10].

Alternatively, ultrasound imaging is another option. Adler et al. [1] used Doppler ultrasound color flow imaging in the study of breast cancer. Abnormalities, masses, architectural distortions, mass shapes, mass margins, and so many other characteristics of breast cancer were observable using this method [23]. Although ultrasound is the option that offers high spatial resolution, and breast tumor angiogenesis is trackable using Doppler flow imaging [47], image contrast is poor in this approach because normal and cancerous tissues each show almost similar acoustical responses to stimuli since both are soft tissue types [15].

More recently, another way of tracking is microwave imaging, which shows good levels of relevancy to diagnose breast cancer in male and female patients [5]. Meany et al. [25] developed a microwave tomography system for experimental breast imaging. Basically, microwave imaging relies on density-based interactions in which dielectric-based interactions are used to detect breast cancer in its early stages. In this approach, dielectric properties of tissues, such as relative permittivity and conductivity, are effective [5, 43]. This imaging scenario, however, provides poor spatial resolution in biological tissues sampling; the reason for this poor resolution is related to the long wavelength of microwaves [5].

By modifying drawbacks of the pure microwave imaging strategy, microwave-induced thermoacoustic imaging (MITAI) incorporates microwave excitation and ultrasound imaging advantages [43]. In the past two decades, this technique has attracted a lot of attention and many scholars are investigating the different aspects of this technique. Kruger et al. [21] performed thermoacoustic computed tomography (CT) with 434 MHz radio waves in five patients with documented breast cancer. They were looking for contrast enhancement of the performed images. Pramanik et al. [29] have developed a novel scanner for breast cancer detection, integrating both thermoacoustic and photoacoustic techniques to achieve dual contrast (microwave and light absorption) imaging. Guo et al. [15] offered a multi-frequency MITAI layout for detecting breast cancer in early stages. Nie et al. [26] developed a system with 1.2 GHz and proved the feasibility of foreign body detection using MITAI. Gong et al. [14] used a 2.45-GHz microwave generator with pulse energy of 2.5 mJ and a duration of 0.5 μ s. Xie et al. [42] and Wang et al. [41] presented simulation works with finite-difference time-domain (FDTD) tools in which they performed the

microwave-induced thermoacoustic simulation in two steps. The first step determines the specific absorption rate (SAR) by using electromagnetic field stimulation. The second step finds the acoustic wave simulation by using SAR distribution from the previous step as the acoustic pressure source. Song et al. [38] developed a hybrid simulation method by combining a finite integration time domain (FITD) method and pseudo-spectral time domain (PSTD) method, which was fast and efficient. Furthermore, by using some real breast tissue, they performed TAI experimentally. They demonstrated the feasibility and effectiveness of both numerical simulations and experimental results. George et al. [13] studied the feasibility of a low-cost and low-power microwave source to generate pressure variations with low-temperature variation by simulating TAI in COMSOL Multiphysics software. Kam et al. [20] investigated on a one-step simulation study of the generation and propagation of thermoacoustic waves in a two-dimensional enclosure using a finite-difference Lattice–Boltzmann-type method (FDLBM), with a single relaxation time and one equilibrium particle distribution function, and a direct aeroacoustic simulation technique that solves the primitive Navier–Stokes equations. Xu et al. [44] investigated a new application of thermoacoustic tomography (TAT) for human finger joints and bones. In their feasibility study, they validated the use of a TAT scanner on a volunteer's joints and bones. Ding et al. [9] designed a microwave-excited ultrasound (MUI) and thermoacoustic dual imaging system. In their system, the piezoelectric transducer used for thermoacoustic signal detection will also emit a highly directional ultrasonic beam. Yongsheng et al. [8] have performed a comprehensive review on MITAI. They reviewed the development of the TAI technique, its excitation source, data acquisition system, and biomedical applications.

Based on the best knowledge of the authors and the abovementioned literature review, very few studies have been conducted concerning issues relevant to three-dimensional simulation of the MITAI process. The simulation process, mentioned in this paper, can consistently solve the whole problem of MITAI process. Three-dimensional simulation can depict all the physics involved in TAI in detail, as a whole, and can be used to estimate the amount of pressure production as a result of this kind of imaging. The purposes of this simulation are to investigate the potentialities of the MITAI process by locating tumor inside different breast tissue types (the normal breast tissue is categorized into three different tissue types including fibro-connective/glandular, transitional, and fatty tissues), to investigate the capability of the MITAI process with respect to the tumor size (different tumor size including 0.5, 1, 2, and 4 cm are considered), and finally to determine the suitable irradiation power level needed for stimulation of the tissue to obtain several kPa of acoustic pressure variation. This acoustic pressure variation must be strong

enough to be detected by transducers for taking an effective image of the tissue. To achieve these purposes, the temperature variation (due to absorption of microwave pulses) and the variation of acoustic pressure (due to temperature variation) are simulated. Because of the multi-physical nature of the objective, both electromagnetic heating and thermal expansion of biological tissue are considered, though thermal expansion is modeled in a single step. Subsequently, the pressure variation field obtained in the tissue is considered as a consequence of such electromagnetic heating. All the simulations are performed with commercial software, COMSOL Multiphysics.

2 Material and methods

This section is divided into six subsections. First, the MITAI technique is clearly explained. Then, governing equations are mentioned, which describe thermoacoustic phenomena with mathematical models. The remaining subsections include necessary information for different steps of the numerical procedure.

2.1 MITAI technique

In MITAI technique, both tumorous and healthy tissues are irradiated by a short pulsed microwave source. The relatively long microwave wavelength (2.45 cm at 2.45 GHz) illuminates the tissue homogeneously [43]. Consequently, the biological tissue undergoes expansion due to the upshot heat fluxes, which are generated as a consequence of microwave radiation absorption and take place near the tissue of interest. Intermittent generated heat flux generated by the pulsed radiation field causes a kind of pressure

variation contour in the microenvironment of the tissue (Fig. 1). Such a thermoelastic pressure wave launched in the tissue can propagate away from the absorbing tissue in all directions. The thermoacoustic signals produced due to thermoelastic expansion demonstrate that the signals are detectable by means of a wideband ultrasonic transducer [43]. However, the amount of microwave absorption mainly depends on the dielectric property of the material and is very different in normal and cancerous tissues [42]. Therefore, the pressure variation produced in normal tissue differs from the one generated as a result of cancerous tissues.

2.2 Mathematical modeling and numerical methodology

The thermoacoustic phenomenon consists of two processes: the absorption of microwave energy and the generation of acoustic waves [46].

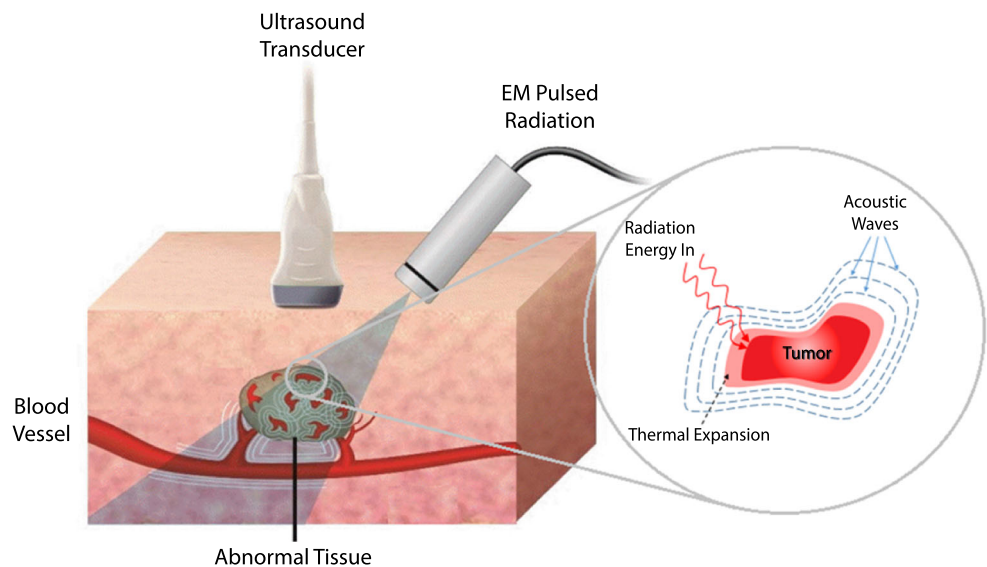
The SAR is the time-averaged rate of energy absorbed per unit volume of the human body, divided by the mass of the volume (W/kg) inside an absorber when tissue is under radio frequency wave [17] and defined as follows [17, 46]:

$$SAR(\vec{r}, t) = \frac{\sigma(\vec{r}) |\vec{E}(\vec{r})|^2}{2\rho(\vec{r})} I(t) \tag{1}$$

where $\sigma(\vec{r})$ is conductivity of the biological tissue, $|E|$ is the amplitude of electric field intensity, ρ is mass density, $I(t)$ is the envelope of instantaneous power of the signal, t is time, and r represents the spatial location of the absorber.

The acoustic wave is generated due to heat generation and thermoelastic expansion, which occurs as a result of

Fig. 1 A schematic of the thermoacoustic phenomenon



microwave energy absorption (described by *SAR*) and is governed by the following two equations [4, 36, 43]:

$$\rho \frac{\partial}{\partial t} u(r,t) = -\nabla p(r,t) \quad (2)$$

$$\nabla \cdot u(r,t) = -\frac{1}{\rho c^2} \frac{\partial}{\partial t} p(r,t) + \alpha p(r,t) + \beta \frac{\partial}{\partial t} T(r,t) \quad (3)$$

where $u(r,t)$ is the acoustic velocity vector, $p(r,t)$ is the acoustic pressure field, ρ is mass density, α is the attenuation coefficient, β is the thermal expansion coefficient, and $T(r,t)$ is temperature.

Because the thermal diffusion time is much higher than the microwave pulse's duration, thermal diffusion can be neglected [46], and the thermal equation can be written as follows:

$$c_p \frac{\partial}{\partial t} T(r,t) = SAR(r,t) \quad (4)$$

where c_p is the specific heat, replacing Eq. (4) into Eq. (3) gives the following:

$$\nabla \cdot u(r,t) = -\frac{1}{\rho c^2} \frac{\partial}{\partial t} p(r,t) + \alpha p(r,t) + \frac{\beta}{c_p} SAR(r,t) \quad (5)$$

So, with solving the Eq. (5), the pressure gradient is obtained. This pressure gradient leads to generation of the acoustic wave.

For numerical modeling, first, the electromagnetic field is simulated. The temperature increase in normal and tumorous tissues is obtained by absorbing this electromagnetic field. Subsequently, acoustic pressure produced in the tissues (due to the increased temperature)

is numerically obtained. In this investigation, a normal breast tissue consisting of three different tissue types with a tumor, which is placed inside of a tank containing castor oil, is simulated. The normal breast tissue types considered are the following: (1) fibro-connective/glandular tissue, (2) transitional tissue, and (3) fatty tissue. These items are irradiated by 1 ms pulsed microwave energy. In order to get a faster computational response, a half-tank full of castor oil is used in which a half-microwave oven waveguide (MOW) is attached to the bottom of the tank (Fig. 2). One of the reasons for choosing castor oil as the immersion medium is to increase the electromagnetic wavelengths produced inside of the tank. This reason and its favorable effect are explained in detail in Sect. 3.1. The other reason is to improve the match between interior and exterior of the breast [3, 33]. So, the losses of electromagnetic field due to refraction at the boundary of the breast tissue would be less. Furthermore, castor oil is minimally dispersive over the frequency range of interest and has low loss [34]. Also, as mentioned in Sill et al.'s study [33], castor oil or in general vegetable oil provides excellent tumor detection and localization in microwave imaging.

Simulations were done with the use of COMSOL Multiphysics software. By coupling “electromagnetic waves (frequency domain)” and “heat transfer in solid” physics, the electromagnetic field was simulated and the temperature increase in normal tissue and tumor, by absorbing this electromagnetic field, was first obtained. Subsequently, by coupling heat transfer in solid and “solid mechanic properties” physics, the acoustic pressure (produced in the tissue due to the

Fig. 2 Three-dimensional view of waveguide, tank, breast tissue, and tumor (baseline model)

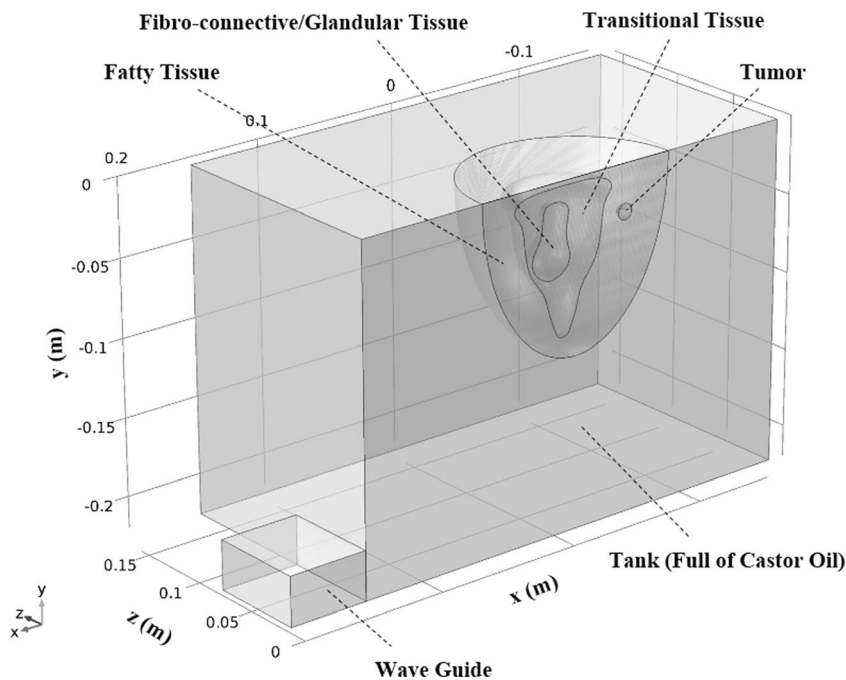
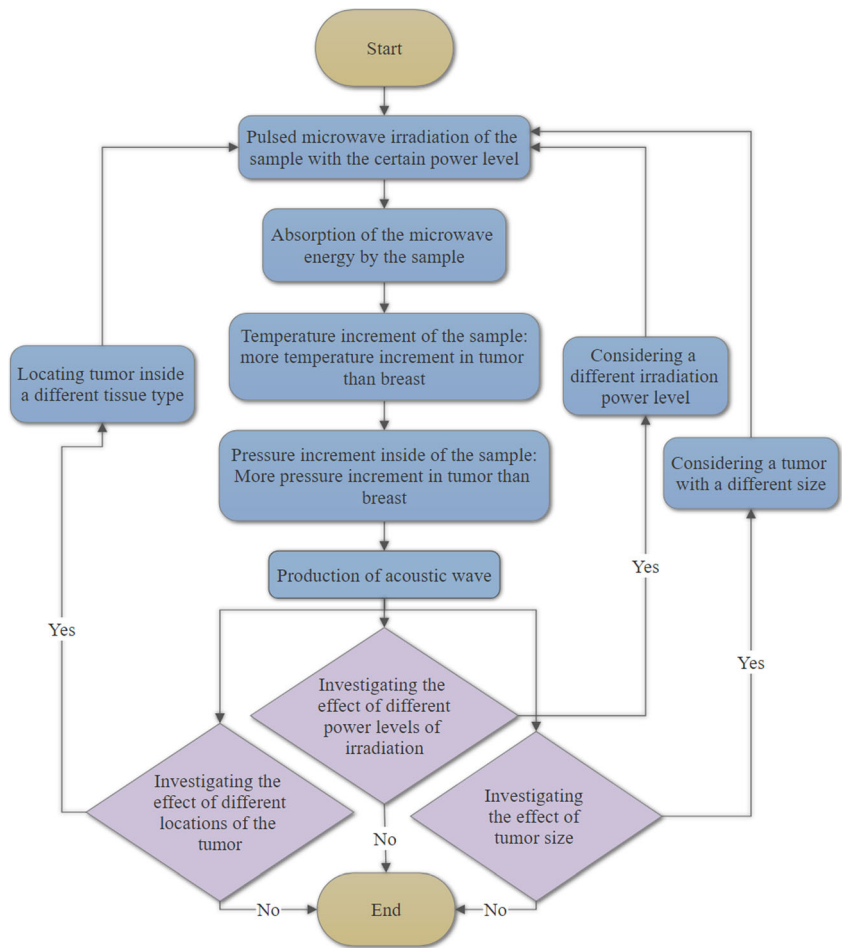


Fig. 3 Step-by-step description of the procedure of the MITAI process and the simulations



increased temperature) was numerically obtained. All simulations are performed via an Intel Core i7 Processor (8M cache, 2.66 GHz) and 12 GB DDR4 RAM system. The simulation time for each case is around 60 to 70 min.

For a better conception of the MITAI process and the procedure of the simulations, a schematic flowchart is illustrated in Fig. 3. In this flowchart, thermoacoustic phenomenon in the MITAI process is elaborated step by step in detail.

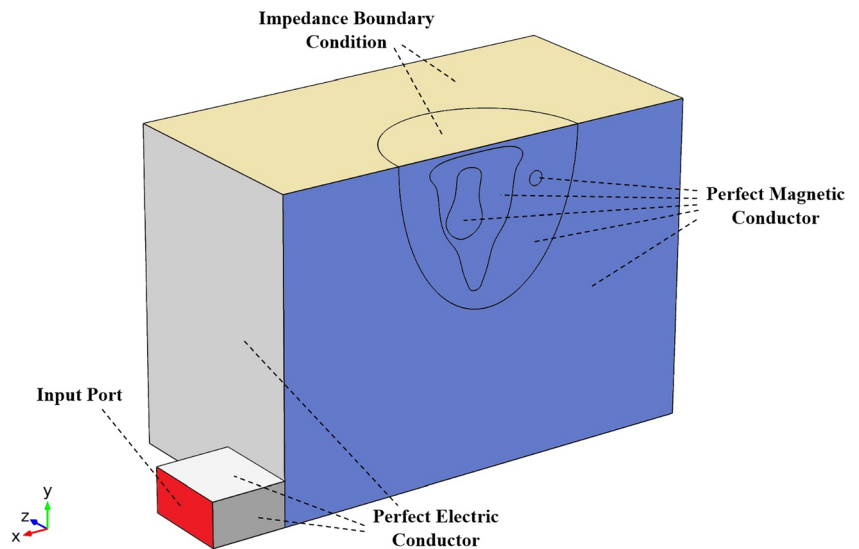
2.3 Geometric model

The region of interest’s geometry, to evaluate waveguide response, has the dimension of $54 \times 32 \times 59 \text{ mm}^3$ [28]. This waveguide operates at the frequency of 2.45 GHz and TE₁₀ mode, which signifies that all electric fields are transverse to the direction of propagation and that no longitudinal electric field is presented. For a rectangular waveguide, the dominant

Table 1 Simulated samples and their different specifications

Sample name	Location of tumor	Diameter of tumor (cm)	Irradiation power (W)
L1	Inside of fibro-connective/glandular tissue	1	1000
L2	Inside of transitional tissue	1	1000
L3 (baseline model)	Inside of fatty tissue	1	1000
S0.5	Inside of fatty tissue	0.5	1000
S2	Inside of fatty tissue	2	1000
S4	Inside of fatty tissue	4	1000
P6000	Inside of fatty tissue	1	6000
P12000	Inside of fatty tissue	1	12,000
P18000	Inside of fatty tissue	1	18,000
P24000	Inside of fatty tissue	1	24,000

Fig. 4 Electromagnetic boundary conditions in baseline model



mode (the mode having the lowest cutoff frequency) is the TE_{10} mode. The half-tank geometry's dimension considered is $313 \times 220 \times 158 \text{ mm}^3$. The breast is considered a quarter of an ellipsoid with semi-axes of $70 \times 110 \times 70 \text{ mm}^3$ and is located inside the tank from the top boundary. The tumor consists of a hemisphere and is located inside the breast, as shown in Fig. 2. In these simulations, the variation of material properties is investigated. In order to simulate samples that have the most similarities to real ones, breast tissue is categorized into three different tissue types including fibro-connective/glandular tissue, transitional tissue, and fatty tissue [45]. The geometry of different tissue types are considered in order to be as similar as possible to the real samples (as shown in Fig. 2). In these simulations, the effect of tumor location, tumor size, and irradiation power levels are investigated. For a better

understanding of the simulated samples, these samples are named and their different specifications are shown in Table 1.

Simulated samples can be categorized into three groups as shown in Table 1. The first group are samples which have prefix L in their names. These samples have different tumor locations but identical tumor size and irradiation power level. The second group are samples with prefix S which have different tumor sizes but identical tumor location and irradiation power level. The third group are samples with prefix P which have different irradiation power levels but identical tumor size and location.

2.4 Boundary conditions

Figure 4 demonstrates the electrical boundary conditions in L3 sample. A symmetrical boundary condition is used for simulation of only half of the whole geometry. These boundaries are considered as a “perfect magnetic conductor.” The above boundary, shown in Fig. 4, is considered an “impedance boundary condition.” The properties of each material (fatty tissue and castor oil) are given for each of the above boundaries because one side of the geometry is an open sided area. The other boundaries are made up of copper

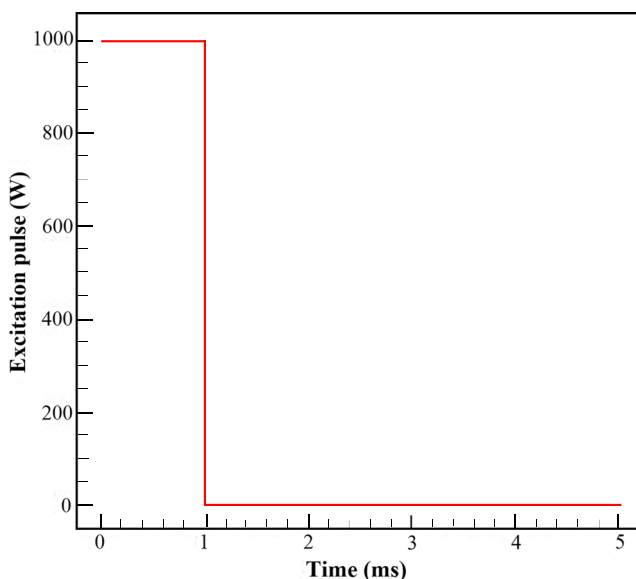


Fig. 5 Excitation pulse of 1000 W, 1 ms plot used for simulation with piecewise function

Table 2 Measured dielectric properties of ex vivo female breast and castor oil [22, 31, 42, 45]

Materials	Dielectric properties	
	Relative permittivity	Electrical conductivity (S/m)
Fibro-connective/glandular tissue	47	2.2
Transitional tissue	20	1
Fatty tissue	7	0.5
Tumor tissue	55	4
Castor Oil	5	$10e-12$

Table 3 Acoustic and thermal parameters for tissues [2, 6, 7, 12, 16, 24, 39, 40, 42]

Tissue types	ρ (kg/m ³)	C_p (J/kg °C)	YM (Pa)	K (W/m K)	ν	α (1/K)
Fibro-connective/glandular	1050	3770	50e+03	0.48	0.49	4.5e-05
Transitional	990	3270	34e+03	0.345	0.49	3.75e-05
Fatty	930	2770	18e+03	0.21	0.49	3e-05
Tumor	1050	3852	106e+03	0.54	0.49	6.5e-05

material and are considered as a “perfect electric conductor” (except the entrance side of the waveguide, which is considered as an input port of microwave energy). All of these boundary conditions are shown in Fig. 4.

The excitation source for microwaves is shown in Fig. 5, with a piecewise function of time that produces a 1-ms pulse with a power of 1000 W. In these simulations, the temperature increase and, in the result of that, the produced pressure due to thermal expansion were obtained after 1 ms for several input power levels (1 kW, 6 kW, 12 kW, 18 kW, and 24 kW).

Dielectric properties, thermal and acoustic parameters for different normal breast tissues and tumor along with castor oil are shown in Table 2. Also, thermal and acoustic parameters for these materials are demonstrated in Table 3. To analyze the results of the simulation, three points are considered on the symmetrical boundary surface for baseline model. The first point is on the fatty tissue at 5 mm distance from the interface. The second point is on the tumor and at the same distance from the interface. The last point is placed exactly on the interface (Fig. 6).

In Table 3, ρ is density, C_p is specific heat, YM is Young’s module, K is thermal conductivity, ν is Poisson’s ratio, and α is the coefficient of thermal expansion.

2.5 Optimum grid generation

In order to examine grid independency, several versions of the computational mesh are generated and applied to the model L3, and then the maximum temperature variation inside the tumor is obtained. A suitable number of cells are selected by a trade-off between the computing resources cost and the

simulation results. When the finer grids do not change the numerical results, the most refined grid is considered to achieve an appropriate grid independency level. This mesh study is done for a 1-ms pulse with 1000 W power for baseline model. The results are shown in Fig. 7.

According to Fig. 7, with increasing the number of grids, the maximum temperature difference in the tumor reaches an almost constant value. On the other hand, Table 4 shows the quantitative values and differences (error between them) of various grid generations in order to select the optimum one. In Fig. 7 and Table 4, the temperature for case 4 and case 5 is approximately the same. So, for decreasing the computational cost, case 4 is selected as the best choice. The optimum grid generation is shown in Fig. 8.

2.6 Validation of the simulation

For validation of simulation results, the increase of temperature at a considered point in the tumor is compared to Georges et al.’s study results [13] by using similar assumptions. Georges et al. [12] have performed a simple 2D simulation of MITAI process. In their simulations, a 2D breast tissue with a tumor within it is considered inside of a waveguide. The geometry dimension of the breast tissue is considered 78×50 mm². They have used an excitation pulse of 200 μ s with different power levels and investigated the amount of temperature increase inside of the tumor and the breast tissue. By considering their geometries and boundary conditions, it has been tried to compare the results of present study’s simulation approach with theirs. In this comparison, two-dimensional simulations are done for 700 W, 7000 W, and 25,000 W input

Fig. 6 Position of considered points to study temperature and pressure variations in magnified baseline model

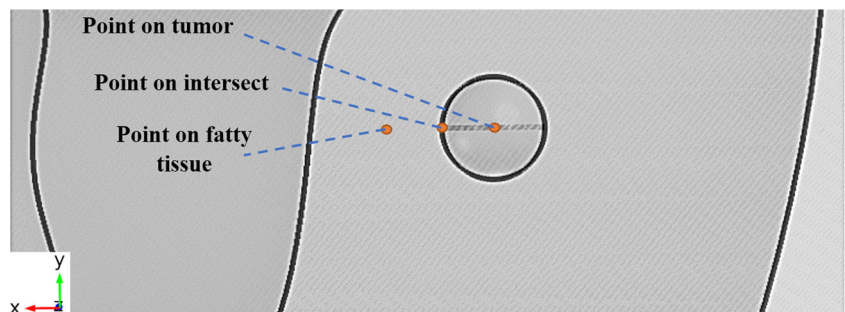
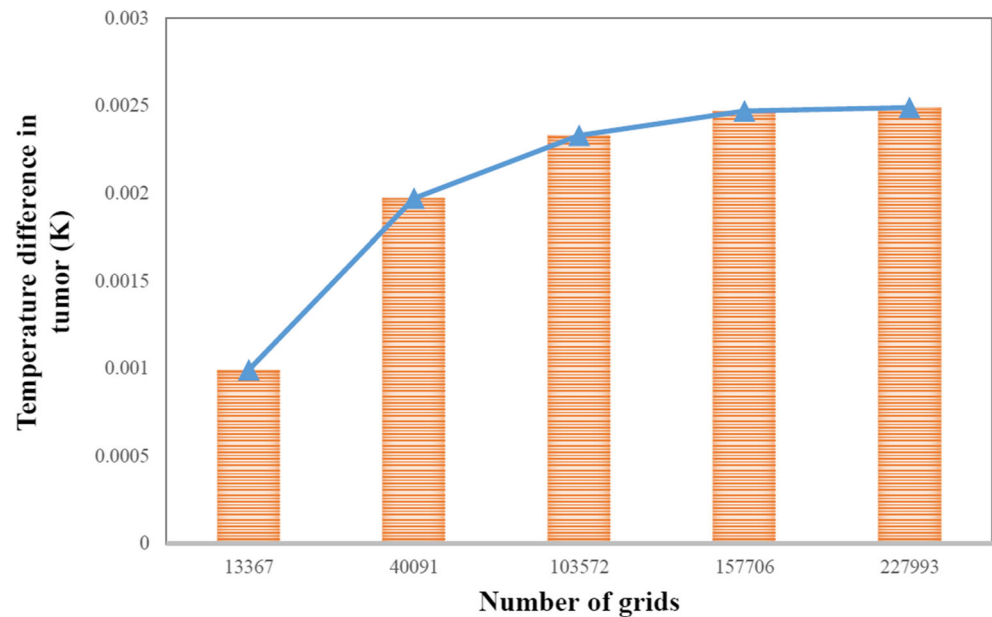


Fig. 7 Grid independency of the current study based on a 1-ms pulse with 1000 W power for baseline model



power levels. The obtained results from the current study, the results of George et al.'s [20] simulations, and the relative error analysis are shown in Table 5.

Table 5 represents that there is an acceptable relative error percentage rate (on average about 5.33%) between the obtained results and George et al.'s simulation results [13].

3 Results and discussion

This section is divided into four subsections. In the first one, for a better demonstration of the MITAI process, distributions of electromagnetic field produced inside of the tank along with distributions of temperature and pressure variations of tissues for sample of L3 (as a baseline model) are shown. For further elucidation, some other results are presented in detail for baseline model, too. In the next subsections, comparative results of

all simulations with respect to tumor location, size, and irradiation power level are investigated in detail.

3.1 Baseline model

An excitation pulse of 1000 W, carried by a 1-ms wave, is used in the TE₁₀ waveguide by consequence of results presented in Fig. 5. For a better conception of this waveguide, Fig. 9 shows the electromagnetic field which is produced inside the tank for 1000 W microwave power after 1 ms when it

Table 4 Quantitative values of various grid generations in order to select the optimum one

Case	Number of grids	Temperature (K)	% Relative error compared to the optimum case
1	13,367	0.000991	59.87
2	40,091	0.00197	20.24
3	103,572	0.00233	5.67
4	157,706	0.00247	–
5	227,993	0.00249	0.8

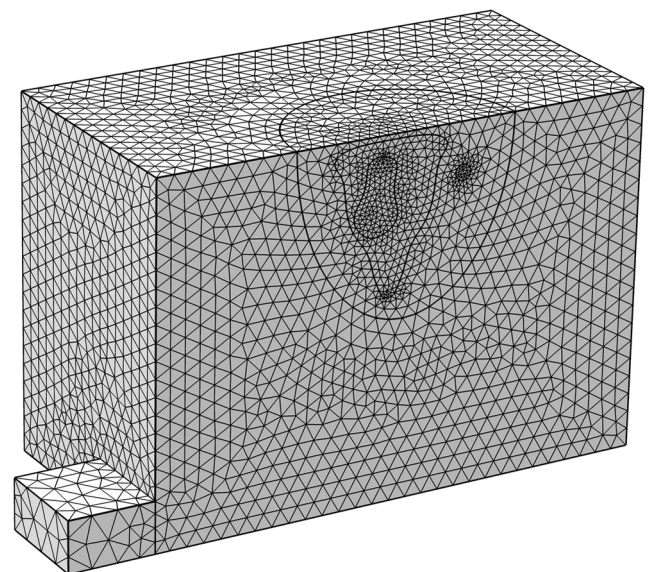


Fig. 8 Optimum grid generation considered

Table 5 Comparison between temperature difference obtained at the tumor and George et al.'s [13] simulation results

	Power (W)	Tumor, ΔT (°C)		% Relative error
		Current study	George et al. [13]	
1	700	0.00155	0.0015	3.33
2	7000	0.01557	0.016	2.68
3	25,000	0.07149	0.065	9.98

is empty. As is shown, the geometrical properties of the tank and waveguide have been properly chosen in order to produce this regular electric field. Figure 9 also demonstrates the amplitude of electric field on the x - y surface, the x - z surface, and the y - z surface which pass through middle of the tank. Figure 9 shows the electromagnetic field produced when the tank is totally empty. Figure 10 indicates the electromagnetic field produced inside the tank when the castor oil, breast tissues, and tumor are considered (for baseline model similar to Fig. 2). The amplitude of electric field on the surfaces introduced above is also illustrated in this figure for an excitation pulse of 1000 W carried by a 1-ms wave. Figure 10 represents that an absolute electric field with a maximum of 2.53×10^4 V/m is produced inside the tank. Both non-malignant

and malignant tissues absorb this microwave energy, but in different levels.

By comparing Figs. 9 and 10, it can be concluded that by adding castor oil, more electromagnetic wavelengths would be produced inside of the tank. The reason is that by changing the immersion medium from air to castor oil, field propagation velocity would be reduced (related to the relative dielectric constant of the medium). This reduction of velocity leads to reduction of wavelength (because the frequency is considered to be constant at 2.45 GHz). This reduction of wave length means that inside of the tank (with a specific length), more electromagnetic wavelengths would be produced. For instance, with air as the immersion medium, we have five peaks of the electromagnetic waves (five wavelengths) produced inside of the tank, but with castor oil this number is changed to 11 (As shown in Figs. 9 and 10). By increasing the electromagnetic wavelengths produced inside of the tank, different parts of the breast tissue would be exposed under approximately the same irradiation. This implies the various temperature increases in different parts of breast are mostly due to the different tissue types, not because of the distance between the tissue and the peak of the electromagnetic field. Figure 11 demonstrates the obtained temperature gradient distribution of different breast tissues and tumor after 1 ms for baseline model.

Figure 11 shows that due to absorption of microwave energy, the temperature is increased in all tissues (maximum

Fig. 9 Electric field amplitude of 1000 W microwave power on different surfaces with an empty tank. **a** Three-dimensional view. **b** x - y surface. **c** x - z surface. **d** y - z surface

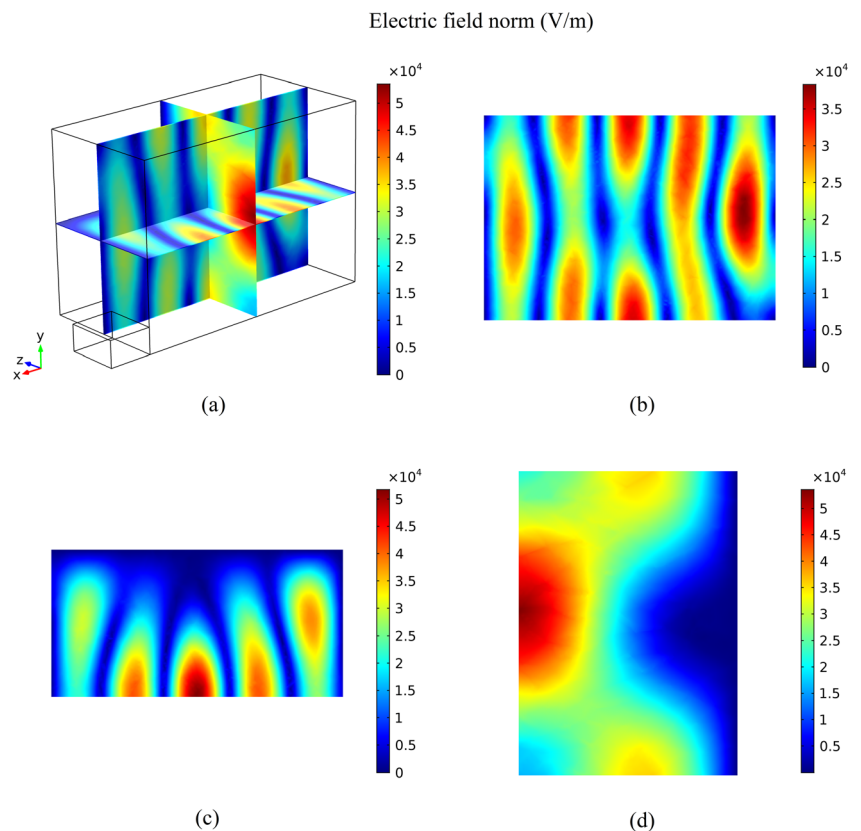
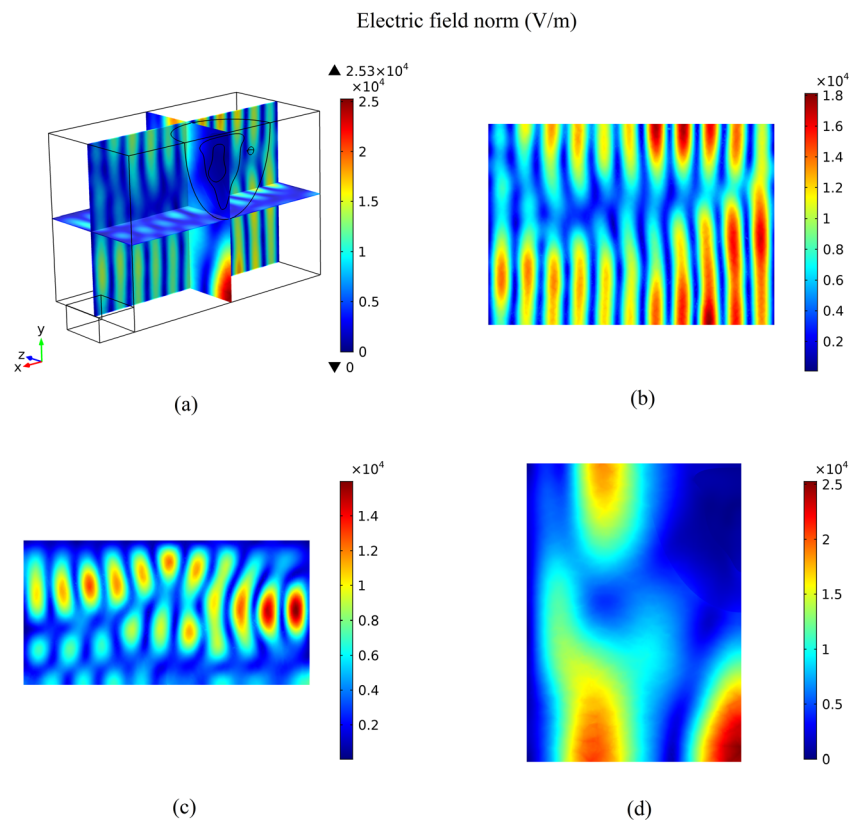


Fig. 10 Electric field amplitude of 1000 W microwave power on different surfaces inside a filled tank (for baseline model). **a** Three-dimensional view. **b** x - y surface. **c** x - z surface. **d** y - z surface



temperature increase is $0.00924\text{ }^{\circ}\text{C}$, due to an excitation pulse of 1000 W, 1 ms). Because of higher dielectric properties of tumor tissue (conductivity 4 S/m and relative permittivity 55) than other breast tissues, which has lower dielectric properties values, the increased temperature in tumor tissue is greater than in all other breast tissues (Fig. 11).

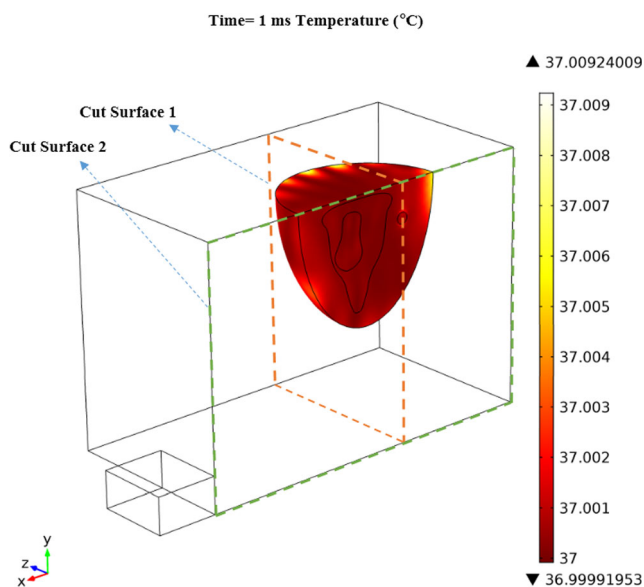


Fig. 11 Temperature gradient distribution of breast and tumor tissues after 1 ms of excitation pulse of 1000 W for baseline model

For further clarity, in Fig. 11, two cut surfaces have been considered. One of them is the x - z surface at $z=0$ mm (the symmetric boundary surface) and the other one is the y - z surface which crosses through the middle of the tumor). Figure 12 shows the temperature gradient distribution at cut surfaces 1 and 2.

Figure 12 represents that the temperature at tumor area is higher than the other parts of the breast tissue. It is because that the dielectric properties of the tumor are higher than other breast tissues (tumor tissue is more condensed than other breast tissues), and it leads to more absorption of electromagnetic energy by the tumor tissue. This more energy absorption by the tumor in comparison with the other parts of the breast leads to more increment in its temperature. Also, Fig. 13 demonstrates the temperature variation over time in different points considered on tumor, fatty tissue, and intersection (as shown in Fig. 6) with a 1000-W, 1-ms pulse for baseline model.

Figure 13 indicates that the temperature increases with a higher gradient at the tumor point compared to other areas because of the high dielectric properties of tumor in comparison to the other tissues. As demonstrated, for an excitation pulse of 1000 W, after 1 ms, the temperature increase in the considered point of the tumor is $0.00056\text{ }^{\circ}\text{C}$ higher than the temperature increase in the considered point of the fatty tissue.

As a result of this additional increase in tumor temperature compared to other parts of the breast tissue, the tumor

Time= 1 ms Temperature (°C)

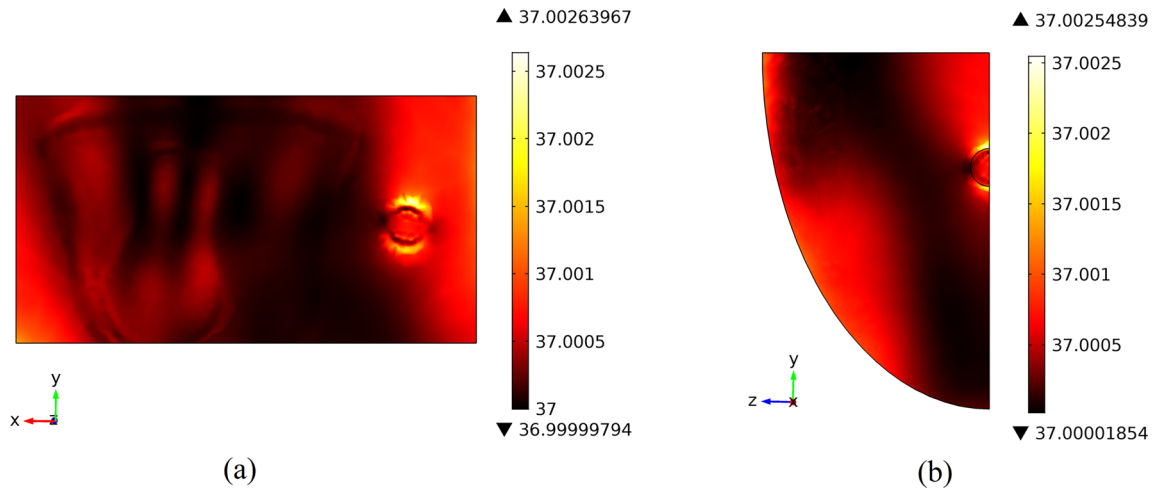


Fig. 12 Temperature gradient distribution of breast and tumor tissues on cut surfaces 1 and 2 for an excitation pulse of 1000 W after 1 ms in baseline model. **a** Cut surface 1. **b** Cut surface 2

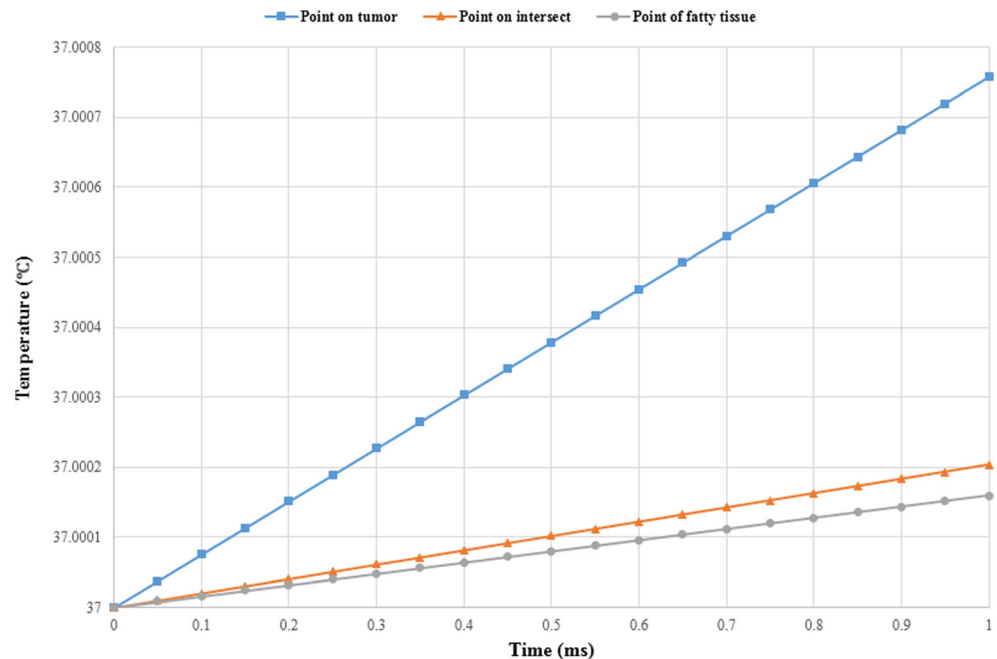
undergoes more expansion than other breast tissues. Because of this additional expansion in tumor tissue, at the intersection between the tumor and fatty tissue, the difference in pressure will be produced (Fig. 14). For further clarity of this pressure gradient, Fig. 15 illustrates the pressure distribution on the cut surfaces mentioned above.

Figures 14 and 15 indicate that tumor undergoes more pressure difference compared to other parts of the breast tissue. The reason is that more temperature increment of the tumor leads to more expansion of the tumor tissue and it leads to production of a higher level of pressure difference at tumor area. These pressure variations produce a pressure wave (an

acoustic wave) that propagates inside the tissue and its surroundings. With the use of an array of transducers, these acoustic waves can be detected and be used for early breast cancer detection. Figure 16 demonstrates the pressure variation over time in different points considered on the tumor, fatty tissue, and intersection, with a 1000-W, 1-ms pulse for baseline model.

Figure 16 shows that variation in amount of pressure over time is higher in the tumor than at the intersection and is higher at the intersection than in the fatty breast tissue. As demonstrated, for an excitation pulse of 1000 W, 1 ms, the pressure variation in the considered point in the tumor is about

Fig. 13 Temperature variation in time at different points with 1000 W, 1 ms pulse for baseline model



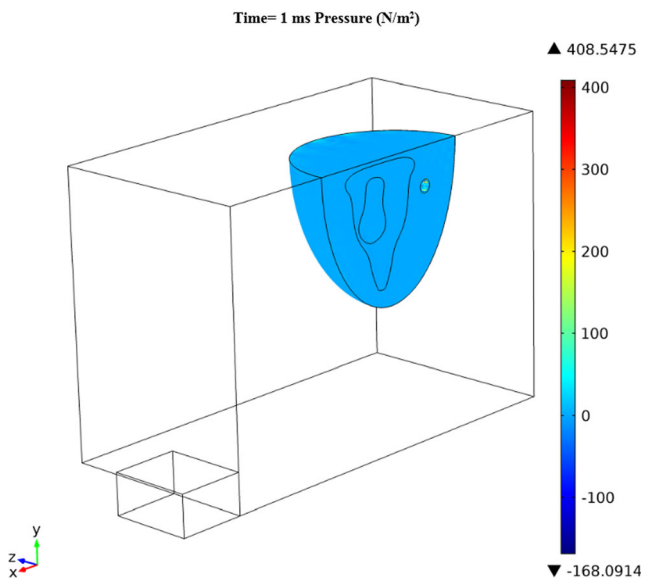


Fig. 14 Pressure gradient distribution of fatty breast and tumor tissues after 1 ms of an excitation pulse of 1000 W for baseline model

13 Pa higher than the pressure variation in the considered point in fatty breast tissue.

3.2 The effect of tumor location

For studying the effect of tumor location on the detection performance of MITAI process, excitation power level and tumor size are considered to be identical in different simulations (including simulation samples L1, L2, and L3). In these simulations, tumor is located inside different breast tissue

types, and then, maximum temperature and pressure variation produced inside of the tumor are evaluated, as illustrated in Fig. 17.

Figure 17 shows that the maximum amount of temperature and also pressure difference inside the tumor is higher in the sample of L3, L2, and L1, respectively. The reason is that the contrast in the microwave-frequency dielectric properties between tumor and normal fatty tissues in the breast is considerable, while this contrast between tumor and normal glandular/fibroconnective tissues is not so much. Difference between tumor and fatty tissue dielectric properties is higher than this difference between tumor and other breast tissues (transitional or fibro-connective/glandular tissues). So, the amount of temperature increases and, in the result of that, pressure increase in tumor and fatty tissue would have a significant difference. Also, this difference of temperature and pressure increases would be higher between tumor and transitional tissues than tumor and fibro-connective/glandular tissues. Therefore, it can be concluded that if tumor locates in the fatty tissue of breast, it would be detected more easily than the condition that tumor locates in the transitional tissue. Also, it would be detected more easily if the tumor locates in the transitional tissue than the fibro-connective/glandular tissue. For instance, the excitation pulse of 1000 W, 1 ms, can produce the maximum pressure difference of 0.584 kPa in tumor when it is located inside fatty tissue, while the same excitation pulse can produce 0.045 kPa in tumor when it is located inside fibro-connective/glandular tissue. It should be noted that the higher produced pressure difference means that it can be detected using array of transducers more easily.

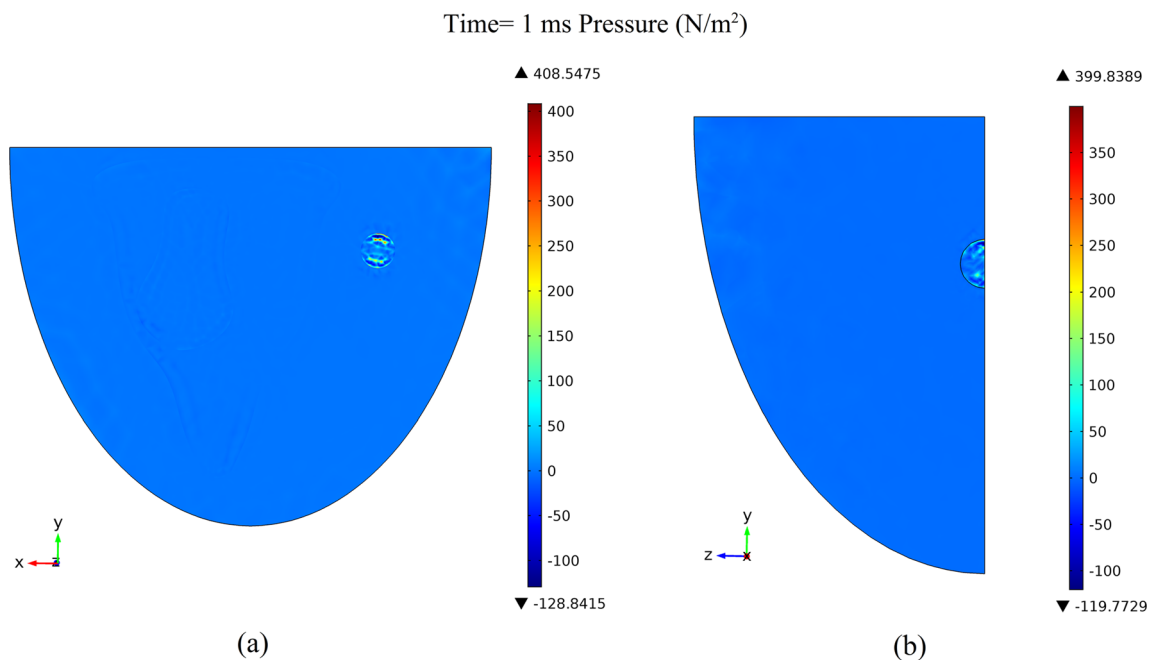
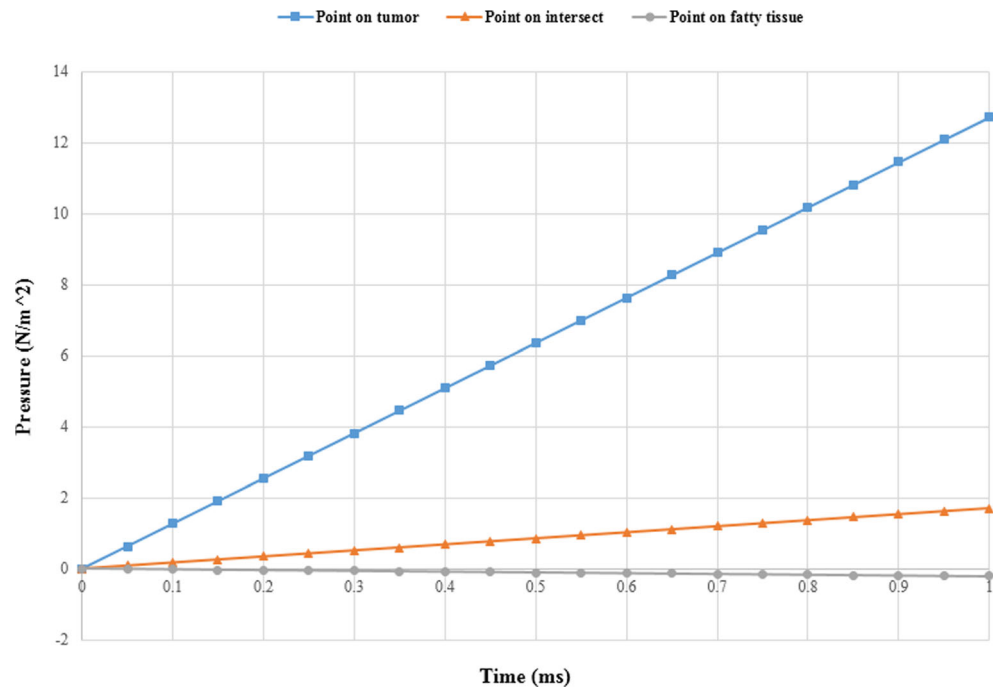


Fig. 15 Pressure gradient distribution of fatty breast and tumor tissues on cut surfaces 1 (a) and 2 (b) for excitation pulse of 1000 W after 1 ms in baseline model. **a** Cut surface 1. **b** Cut surface 2

Fig. 16 Pressure variation in time at different points with 1000 W, 1 ms pulse for baseline model



3.3 The effect of tumor size

For investigating the effect of tumor size on the detection performance of MITAI process, excitation power level and tumor location are considered to be identical in different simulations (including simulation samples S0.5, L3, S2, and S4), while tumor size is assumed to be changed. Tumors with different diameters of 0.5, 1, 2, and 4 cm are considered. These sizes are considered according to different stages of cancer development [32, 35, 37]. The variation of maximum temperature and pressure differences produced inside of the tumor is evaluated for each of the mentioned samples, as illustrated in Fig. 18.

Figure 18 demonstrates that by increasing the tumor size, the increase of temperature in tumor will be higher. Therefore, the bigger the tumor, the greater the increased temperature. On the other hand, it is obvious that higher temperature increase leads to higher pressure production. So, as shown in Fig. 18, by increasing the tumor size, the pressure difference is greater. Therefore, the bigger the tumor, the greater amplitude of the produced acoustic wave. The reason is that, by increasing tumor size, the tumor mass which can absorb electromagnetic energy is increased. So, a bigger tumor would absorb more energy than smaller ones. This leads to a more temperature increase and, also, more pressure increase inside tumor. Also,

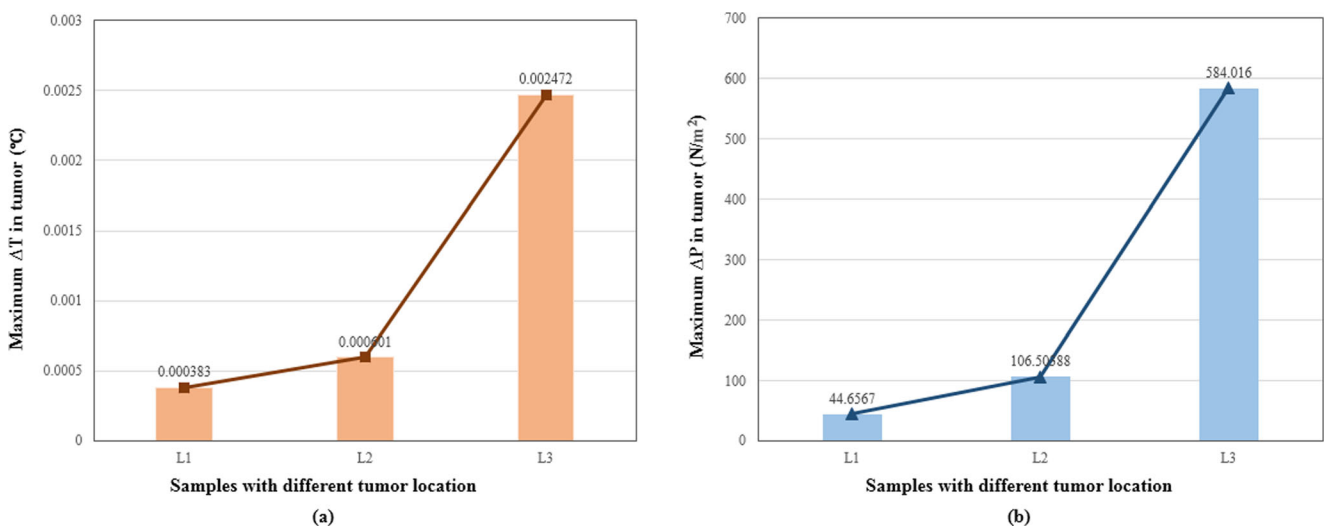


Fig. 17 The variation of maximum temperature and pressure differences produced inside of the tumor tissue for investigating the effect of tumor location. **a** Maximum temperature difference. **b** Maximum pressure difference

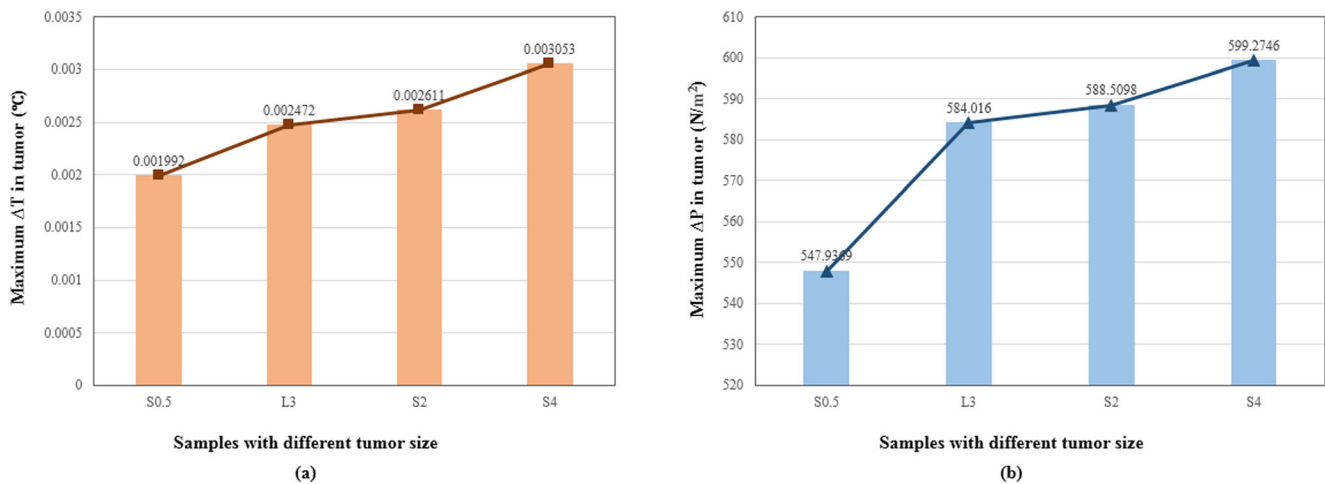


Fig. 18 The variation of maximum temperature and pressure differences produced inside of the tumor tissue for investigating the effect of tumor size. **a** Maximum temperature difference. **b** Maximum pressure difference

it can be mentioned that tumor size does not have a major effect on the amount of pressure increase in tumor. Actually, by increasing the tumor diameter from 0.5 to 4 cm, the amount of maximum pressure variation produced in tumor only changed from 0.548 to 0.599 kPa. Thus, it can be concluded that MITAI process is a powerful imaging technique for detecting breast tumors in early stages of cancers and the tumor size does not play a major role on detection performance of MITAI process.

3.4 The effect of irradiation power level

To study the effect of irradiation power level, tumor location and size are considered to be identical in different simulations (including simulation samples L3, P6000, P12000, P18000, and P24000), while only irradiation power is assumed to be changed. Irradiation power levels of 1000, 6000, 12,000, 18,000, and 24,000 W are considered. The maximum

temperature and pressure variation produced inside of the tumor are evaluated for each of these samples between the times of before excitation and 1 ms after excitation, as shown in Fig. 19.

Figure 19a demonstrates that by increasing the excitation power level, the increase of temperature will be higher. Therefore, the higher the excitation power level, the greater the increased temperature. The reason is that by increasing the excitation power level, breast and tumor tissues will be irradiated by a higher electromagnetic energy and so more energy will be absorbed by both tissues. This increase in the amount of energy absorption leads to a higher increment of temperatures in the tissues. Figure 19b represents that by increasing the excitation power level, the increase of temperature will be higher, and so, the pressure difference will be greater. Therefore, the higher the excitation power level, the greater amplitude of the produced acoustic wave. For instance, the excitation pulse of 1000 W, 1 ms, can lead to production of

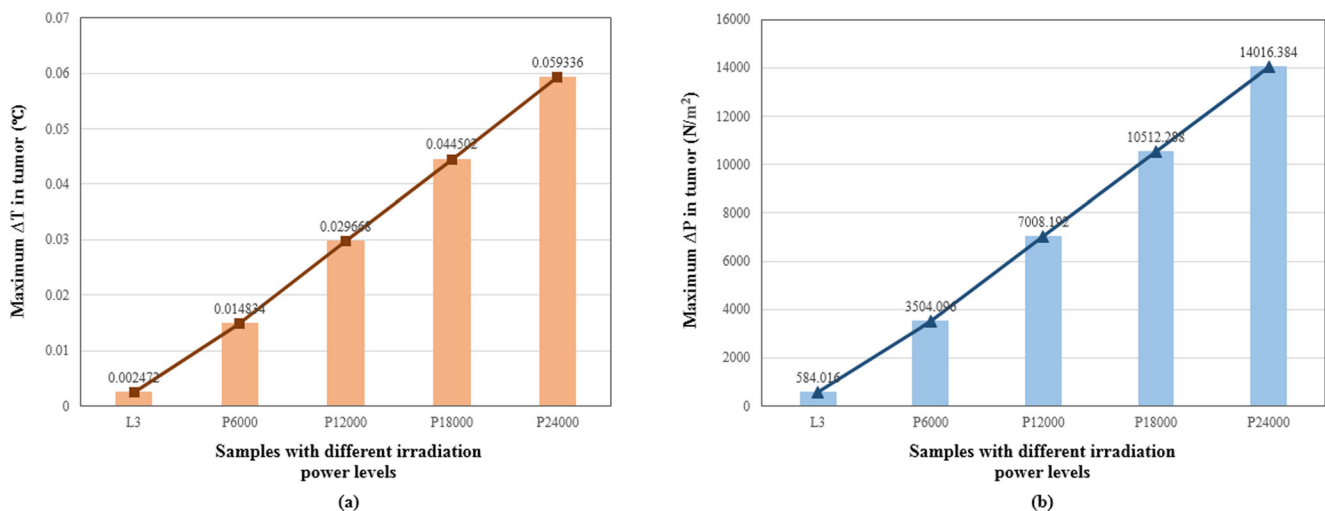


Fig. 19 The variation of maximum temperature and pressure differences produced inside of the tumor tissue for investigating the effect of irradiation power levels. **a** Maximum temperature difference. **b** Maximum pressure difference

maximum 0.584 kPa pressure difference inside the tumor, while the excitation pulse of 6000 W, 1 ms, can produce a maximum 3.504 kPa pressure difference in tumor.

4 Conclusions

Thermoacoustic imaging can be considered as one of the current alternatives for detection of breast cancer in early stages. This technique incorporates microwave excitation and ultrasound imaging advantages. The thermoacoustic phenomenon consists of two parts: temperature increase (due to the absorption of microwave energy and expansion) and pressure production (due to the temperature increase). In the current study, the capability of a three-dimensional mathematical simulation, which can solve the whole problem of the thermoacoustic phenomenon consistently, is investigated. For this purpose, some of this study's results are first compared to other research studies mentioned in the literature (for verification of the simulation procedure) and then several three-dimensional models (for investigating the effects of tumor location and size under different power levels of electromagnetic irradiation) are considered. Maximum temperature and pressure variation at tumor are then obtained. Results show that a small variation in tumor temperature leads to production of several kilopascals of pressure variations. Such minuscule values cannot cause any tissue damage. However, because of these pressure variations, acoustic waves are produced. These waves can be detected with an array of transducers and then used for image construction. Results of the present study with respect to tumor location and size and also irradiation power level can be outlined as follows:

- Tumor location has a major effect on the detecting performance in MITAI method.
- If tumor locates in the fatty tissue of breast, it would be much easier to detect it than the condition that tumor locates in the transitional tissue. Also, it would be detected more easily if the tumor locates in the transitional tissue than the fibro-connective/glandular tissue.
- Increasing tumor size will make it easier to be detected.
- Tumor size plays a minor role on the detecting performance of MITAI technique.
- MITAI technique can be used for detecting tumors with diameters even as small as 0.5 cm. So, it is a powerful tool for detecting breast cancers in early stages.
- The higher the excitation power level, the greater the amplitude of the produced acoustic wave. So, the detection of tumors becomes easier.

Results obtained from this research study model show that TAI is a powerful tool for detecting cancer in tissues. This method can be employed for determination of the amount of

pressure variation produced, the acoustic pressure magnitude, and for much more complicated geometries. TAI can also be a helpful tool for simulating real and experimental samples.

References

1. Adler DD, Carson PL, Rubin JM, Quinn-Reid D (1990) Doppler ultrasound color flow imaging in the study of breast cancer: preliminary findings. *Ultrasound Med Biol* 16:553–559. [https://doi.org/10.1016/0301-5629\(90\)90020-D](https://doi.org/10.1016/0301-5629(90)90020-D)
2. Ahmadian MT, Nikooyan AA (2006) Modeling and prediction of soft tissue directional stiffness using in-vitro force displacement data. *Int J Sci Res* 16:385–389
3. Baran A, LoVetri J, Kurrant D, Fear E (2017 XXXIInd, 2017. IEEE) Immersion medium independent microwave breast imaging. In: General Assembly and Scientific Symposium of the International Union of Radio Science (URSI GASS), pp 1–4
4. Bazmara H, Soltani M, Sefidgar M, Bazargan M, Naeenian MM, Rahmim A (2016) Blood flow and endothelial cell phenotype regulation during sprouting angiogenesis. *Med Biol Eng Comput* 54: 547–558
5. Bindu G, Lonappan A, Thomas V, Aanandan CK, Mathew KT (2006) Active microwave imaging for breast cancer detection. *Prog Electromagn Res* 58:149–169
6. Channugam AS, Hatwar R, Herman C (2012) Thermal analysis of cancerous breast model. In ASME International Mechanical Engineering Congress and Exposition, Proceedings (IMECE) 2: 135–143. <https://doi.org/10.1115/IMECE2012-88244>
7. Chen EJ, Novakofski J, Jenkins WK, O'Brien WD (1996) Young's modulus measurements of soft tissues with application to elasticity imaging. *IEEE Trans Ultrason Ferroelectr Freq Control* 43:191–194
8. Cui Y, Yuan C, Ji Z (2017) A review of microwave-induced thermoacoustic imaging: excitation source, data acquisition system and biomedical applications. *J Innov Opt Health Sci* 10:1730007
9. Ding W, Ji Z, Xing D (2017) Microwave-excited ultrasound and thermoacoustic dual imaging. *Appl Phys Lett* 110:183701
10. Elmore JG, Barton MB, Mocerri VM, Polk S, Arena PJ, Fletcher SW (1998) Ten-year risk of false positive screening mammograms and clinical breast examinations. *N Engl J Med* 338:1089–1096. <https://doi.org/10.1056/NEJM199804163381601>
11. Ferlay J, Soerjomataram I, Dikshit R, Eser S, Mathers C, Rebelo M, Parkin DM, Forman D, Bray F (2015) Cancer incidence and mortality worldwide: sources, methods and major patterns in GLOBOCAN 2012. *Int J Cancer* 136:E359–E386. <https://doi.org/10.1002/ijc.29210>
12. Gefen A, Dilmoney B (2007) Mechanics of the normal woman's breast. *Technol Health Care* 15:259–271
13. George T, Rufus E, Alex ZC (2015) Simulation of microwave induced thermoacoustical imaging technique for cancer detection. *ARNP J Eng Appl Sci* 10(20): 9424–9428
14. Gong W, Chen G, Zhao Z, Nie Z (2009) Estimation of threshold noise suppression algorithm in microwave induced thermoacoustic tomography. Paper presented at the Asia Pacific Microwave Conference, Singapore, 2009, pp. 653–656. <https://doi.org/10.1109/APMC.2009.53>
15. Guo B, Li J, Zmuda H, Sheplak M (2007) Multifrequency microwave-induced thermal acoustic imaging for breast cancer detection. *IEEE Trans Biomed Eng* 54:2000–2010. <https://doi.org/10.1109/TBME.2007.895108>
16. Holmes KR Thermal conductivity data for specific tissues and organs for humans and other mammalian species. Thermal Properties. <http://users.ece.utexas.edu/~valvano/research/Thermal.pdf>

17. Jin X, Wang LV (2006) Thermoacoustic tomography with correction for acoustic speed variations. *Phys Med Biol* 51:6437–6448. <https://doi.org/10.1088/0031-9155/51/24/010>
18. Jing Z, Niklason L, Stein J, Shaw I, Defreitas K, Farbizio T, Ruth C, Ren B, Smith A (2007) X-ray mammography/tomosynthesis of patient's breast. Patent US7881428B2, issued February 1, 2011. <https://patents.google.com/patent/US7881428B2/en>
19. Johansson I, Ringnér M, Hedenfalk I (2013) The landscape of candidate driver genes differs between male and female breast cancer. *PLoS One* 8:e78299. <https://doi.org/10.1371/journal.pone.0078299>
20. Kam EWS, So RMC, Fu SC (2016) One-step simulation of thermoacoustic waves in two-dimensional enclosures. *Comput Fluids* 140:270–288
21. Kruger RA, Miller KD, Reynolds HE, Kiser WL Jr, Reinecke DR, Kruger GA (2000) Breast cancer in vivo: contrast enhancement with thermoacoustic CT at 434 MHz—feasibility study. *Radiology* 216:279–283
22. Lazebnik M, Popovic D, McCartney L, Watkins CB, Lindstrom MJ, Harter J, Sewall S, Ogilvie T, Magliocco A, Breslin TM (2007) A large-scale study of the ultrawide band microwave dielectric properties of normal, benign and malignant breast tissues obtained from cancer surgeries. *Phys Med Biol* 52:6093–6115
23. Li B, Zhao X, Dai SC, Cheng W (2014) Associations between mammography and ultrasound imaging features and molecular characteristics of triple-negative breast cancer. *Asian Pac J Cancer Prev* : APJCP 15:3555–3559
24. McKnight AL, Kugel JL, Rossman PJ, Manduca A, Hartmann LC, Ehman RL (2002) MR elastography of breast cancer: preliminary results. *Am J Roentgenol* 178:1411–1417
25. Meaney PM, Fanning MW, Reynolds T, Fox CJ, Fang Q, Kogel CA, Poplack SP, Paulsen KD (2007) Initial clinical experience with microwave breast imaging in women with normal mammography. *Acad Radiol* 14:207–218. <https://doi.org/10.1016/j.acra.2006.10.016>
26. Nie L, Xing D, Zhou Q, Yang D, Guo H (2008) Microwave-induced thermoacoustic scanning CT for high-contrast and noninvasive breast cancer imaging. *Med Phys* 35:4026–4032. <https://doi.org/10.1118/1.2966345>
27. Ottini L (2014) Male breast cancer: a rare disease that might uncover underlying pathways of breast cancer. *Nat Rev Cancer* 14:643–644. <https://doi.org/10.1038/nrc3806>
28. Pitchai K (2011) Electromagnetic and heat transfer modeling of microwave heating in domestic ovens. digitalcommons.unl.edu
29. Pramanik M, Ku G, Li C, Wang LV (2008) Design and evaluation of a novel breast cancer detection system combining both thermoacoustic (TA) and photoacoustic (PA) tomography. *Med Phys* 35:2218–2223
30. Rudlowski C (2008) Male breast cancer. *Breast Care* 3:183–189. <https://doi.org/10.1159/000136825>
31. Saied M, Mansour S, El Sabee M, Saad A, Abdel-Nour K (2012) Some electrical and physical properties of castor oil adducts dissolved in 1-propanol. *J Mol Liq* 172:1–7
32. Sefidgar M, Soltani M, Raaheemifar K, Bazmara H, Nayinian SMM, Bazargan M (2014) Effect of tumor shape, size, and tissue transport properties on drug delivery to solid tumors. *J Biol Eng* 8:12
33. Sill J, Fear E (2005) Tissue sensing adaptive radar for breast cancer detection: study of immersion liquids. *Electron Lett* 41:113–115
34. Sill JM, Fear EC (2005) Tissue sensing adaptive radar for breast cancer detection—experimental investigation of simple tumor models. *IEEE Trans Microwave Theory Tech* 53:3312–3319
35. Soltani M (2012). Numerical modeling of drug delivery to solid tumor microvasculature, PhD thesis. Chem Eng (Nanotechnology), Waterloo, Ontario, Canada. <https://uwspace.uwaterloo.ca/handle/10012/7278>
36. Soltani M, Chen P (2011) Numerical modeling of fluid flow in solid tumors. *PLoS One* 6:e20344
37. Soltani M, Chen P (2012) Effect of tumor shape and size on drug delivery to solid tumors. *J Biol Eng* 6:4
38. Song J, Zhao Z, Wang J, Zhu X, Wu J, Nie ZP, Liu QH (2013) An integrated simulation approach and experimental research on microwave induced thermo-acoustic tomography system. *Prog Electromagn Res* 140:385–400
39. Stylianopoulos T, Martin JD, Snuderl M, Mpekris F, Jain SR, Jain RK (2013) Coevolution of solid stress and interstitial fluid pressure in tumors during progression: implications for vascular collapse. *Cancer Res* 73:3833–3841. <https://doi.org/10.1158/0008-5472.CAN-12-4521>
40. Van Houten EE, Doyley MM, Kennedy FE, Weaver JB, Paulsen KD (2003) Initial in vivo experience with steady-state subzone-based MR elastography of the human breast. *J Magn Reson Imaging* 17:72–85
41. Wang X, Bauer DR, Witte R, Xin H (2012) Microwave-induced thermoacoustic imaging model for potential breast cancer detection. *IEEE Trans Biomed Eng* 59:2782–2791. <https://doi.org/10.1109/TBME.2012.2210218>
42. Xie Y, Guo B, Li J, Ku G, Wang LV (2008) Adaptive and robust methods of reconstruction (ARMOR) for thermoacoustic tomography. *IEEE Trans Biomed Eng* 55:2741–2752. <https://doi.org/10.1109/TBME.2008.919112>
43. Xu M, Wang LV (2002) Time-domain reconstruction for thermoacoustic tomography in a spherical geometry. *IEEE Trans Med Imaging* 21:814–822. <https://doi.org/10.1109/TMI.2002.801176>
44. Xu X, Huang L, Ling Y, Jiang H (2017) Thermoacoustic imaging of finger joints and bones: a feasibility study. In: *Proceedings of the 2016 International Conference on Biotechnology & Medical Science*. World Scientific, Singapore, pp 243–248
45. Zastrow E, Zastrow E, Davis SK, Lazebnik M, Kelcz F, Van Veen BD, Hagness SC (2007) Database of 3D gridbased numerical breast phantoms for use in computational electromagnetics simulations. Instruction manual. uwcem.ece.wisc.edu
46. Zhu KG, Popovic M (2009) Spectral difference between microwave radar and microwave-induced thermoacoustic signals. *IEEE Antennas Wirel Propag Lett* 8:1259–1262
47. Zhu Q, You S, Jiang Y, Zhang J, Xiao M, Dai Q, Sun Q (2011) Detecting angiogenesis in breast tumors: comparison of color Doppler flow imaging with ultrasound-guided diffuse optical tomography. *Ultrasound Med Biol* 37:862–869. <https://doi.org/10.1016/j.ultrasmedbio.2011.03.010>
48. Zurrida S, Nolè F, Bonanni B, Mastropasqua MG, Arnone P, Gentilini O, Latronico A (2010) Male breast cancer. *Future Oncol* 6:985–991. <https://doi.org/10.2217/fon.10.55>

Publisher's note Springer Nature remains neutral with regard to jurisdictional claims in published maps and institutional affiliations.



Dr. M. Soltani has completed his PhD at the University of Waterloo and postdoctoral studies at the University of Johns Hopkins. Now, he is the Assistant Prof. at K. N. Toosi University of Technology and the Adjunct Prof. at Waterloo University. His main researches are placed in the field of Biomedical Engineering.



Farshad Moradi Kashkooli is now PhD candidate in mechanical engineering at K. N. Toosi University of Technology. His researches focused on modeling of cancer diagnosis, treatment, and drug delivery. He is also working in different fields of both Mechanical and Biomedical Engineering.



Reza Rahpeima received his BSc degree in Mechanical Engineering from Buali-Sina University in 2015 and his MSc degree in Aerospace Engineering from K. N. Toosi University of Technology in 2018. He has good knowledge in biological system modeling.